# XGBoost-Based Analysis of the Relationship Between Urban 2-D/3-D Morphology and Seasonal Gradient Land Surface Temperature

Xinyue Ma, Jun Yang, Rui Zhang, Wenbo Yu, Jiayi Ren, Xiangming Xiao, and Jianhong Xia

***Abstract*—The escalation of greenhouse gas emissions has led to a continuous rise in land surface temperature (LST). Studies have highlighted the substantial influence of urban morphology on LST; however, the impact of different dimensional indicators and their gradient effects remain unexplored. Selecting the urban area of Shenyang as a case, we chose various indicators representing different dimensions. By employing XGBoost for regression analysis, we aimed to explore the effects of urban 2-D and 3-D morphology on seasonal LST and its gradient effect. The following results were obtained: 1) the spatial pattern of LST in spring and winter in Shenyang was higher in the suburbs than in the center; 2) the correlation patterns of the indicators in spring and winter were similar, except for the proportion of woodland and grass, digital elevation model, and sky view factor, which exhibited opposing trends in summer and autumn; 3) vegetation and construction had the highest influence on LST in the 2-D index, followed by building forms and natural landscapes in the 3-D urban morphology; and 4) the influence of each indicator varied significantly across different gradients. Among all the indicators, the landscape index, social development, building forms, and skyscape had the highest impacts on urban areas. Vegetation and built-up areas had a greater influence on suburban areas. The findings of this study can assist in adjusting urban morphology and provide valuable recommendations for targeted improvements in thermal environments, thereby contributing to urban sustainable development.**

***Index Terms*—2-D/3-D urban morphology, gradient effect, seasonal land surface temperature, XGboost.**

Manuscript received 28 August 2023; revised 10 November 2023 and 12 December 2023; accepted 27 December 2023. Date of publication 1 January 2024; date of current version 8 February 2024. This work was supported in part by the National Natural Science Foundation of China under Grant 41771178 and Grant 42030409, in part by Basic Scientific Research Project (Key Project) of the Education Department of Liaoning Province under Grant LJKZ0964, in part by the Fundamental Research Funds for the Central Universities under Grant N2111003, and in part by the Natural Science Foundation of Guizhou Province under Grant (2019)1150. *(Corresponding author: Jun Yang.)*

Xinyue Ma and Rui Zhang are with Urban Climate and Human Settlements Research' Lab, Jangho Architecture College, Northeastern University, Shenyang 110169, China (e-mail: womaxinyue@163.com; 2101418@stu.neu.edu.cn).

Wenbo Yu and Jiayi Ren are with the School of humanities and law, Northeastern University, Shenyang 110169, China (e-mail: 2110013@stu.neu.edu.cn; 2210011@stu.neu.edu.cn).

Jun Yang is with Urban Climate and Human Settlements Research' Lab, Jangho Architecture College, Northeastern University, Shenyang 110169, China, and also with Human Settlements Research Center, Liaoning Normal University, Dalian 116029, China (e-mail: yangjun8@mail.neu.edu.cn).

Xiangming Xiao is with the Department of Microbiology and Plant Biology, Center for Earth Observation and Modeling, University of Oklahoma, Norman, OK 73019 USA (e-mail: xiangming.xiao@ou.edu).

Jianhong Xia is with the School of Earth and Planetary Sciences (EPS), Curtin University, Perth 65630, Australia (e-mail: c.xia@curtin.edu.au).

Digital Object Identifier 10.1109/JSTARS.2023.3348476

## I. Introduction

SINCE the Second Industrial Revolution, cities have developed rapidly, leading to population growth, increased density, and improvements in quality of life [1], [2], [3], [4], [5]. To fulfill residents' living requirements, significant transformations have occurred in urban morphologies, with a rapid increase in impermeable surfaces, a continuous rise in the number of high-rise structures, and the ongoing expansion of both 2-D and 3-D urban volumes [6], [7], [8], [9], [10]. These urban morphological shifts have heightened the ground's solar energy absorption capacity, elevating land surface temperature (LST) [11], [12], [13], [14]. The Intergovernmental Panel on Climate Change (IPCC) report indicates that greenhouse gas emissions will lead to an unavoidable 1.5 °C temperature rise between 2020 and 2040, resulting in substantial harm to the environment [15], [16], [17], [18]. Remote sensing technology has been utilized to assess urban morphology and thermal environmental changes [19], [20], [21], [22]. Through the combination of remote sensing and GIS, dynamic information, such as urban spatial distribution, impervious water ratio, and building forms, can be obtained and processed, creating a scientific foundation for urban planning and design [23], [24]. Therefore, utilizing remote sensing information to optimize urban morphology in different dimensions is vital for preventing the urban heat island effect and ensuring sustainable development [25], [26].

No standardized definition or measurement method exists for urban morphology [27]. Previous research has focused on macroscale urban morphology, such as urban expansion or compactness, and its impact on LST; however, analyzing microscale urban morphology optimization is also a crucial path of investigation [28], [29], [30]. Given the difficulty of directly representing urban morphology, scholars often use related indicators to quantify urban morphological characteristics, such as landscape patterns, surface roughness, building forms, and socioeconomic development indices [31], [32], [33]. These indices are frequently employed to investigate the influence of urban morphology on LST, air quality, energy usage, and related aspects [34], [35], [36]. However, research on different dimensions of urban morphology is limited.

Research concerning urban morphology-LST relationships has predominantly centered on their correlation. [25], [37], [38], [39]. Guo et al. [40] investigated indices such as landscape patterns, the proportion of construction land (PCL), the proportion

of woodland and grass (PWG), and the normalized difference built-up index (NDBI), identifying a strong correlation between NDBI and LST. Liu et al. [27] explored the influence of different terrains and urban morphologies on summer LST using indices such as the normalized difference vegetation index (NDVI) and digital elevation model (DEM) and observed variations in the impact of different terrains on the urban heat island effect. However, these studies solely evaluated the collective impact of the indices on the city. Previous research has highlighted divergent associations between urban morphology and LST across diverse urban development gradients [42], [43]. Liang et al. [44] found that variations in LST gradients may be attributed to urban areas, population density, and nighttime lights. Moreover, Sun et al. [45] suggested that a decrease in LST with outward urban expansion was influenced more by landscape patterns. Although these studies have demonstrated the practical impact of different indices on gradient variations in LST, the different effects and contributions of various indices across gradients have not been explored [46]. Identifying the dynamic contributions of indices across gradients is crucial for targeted LST regulation, enabling maximum results with minimal inputs, and is essential for the green and sustainable development of cities.

Adoption of the appropriate research methodology is also crucial for such investigations. In current research, regression methodologies predominantly encompass traditional models and machine learning algorithms. While traditional regression techniques, such as multiple linear regression and geographically weighted regression (GWR), adeptly model inter-variable relationships, they are limited by issues including sensitivity to outliers and neglect of spatial autocorrelation [47], [48]. Advances in computing have propelled machine learning to the forefront of regression analysis, with methods like support vector machines (SVM), random forest (RF), boosted regression trees (BRT), and XGBoost gaining prominence [49], [50], [51]. XGBoost, a tree-based ensemble learning approach, leverages multiple decision trees to minimize model bias and, compared to SVM, significantly reduces training time due to its parallel computation and optimized data structures [52], [53]. Unlike RF, XGBoost incorporates regularization to curb overfitting, exhibiting superior performance with complex datasets [54], [55]. BRT serves as the conceptual precursor to XGBoost, which surpasses its predecessor in fitting accuracy, computational efficiency, and handling of missing or zero-inflated data [52]. It can also rank the importance of features and quantify their impact, thereby facilitating an understanding of the contributions of different independent variables [56], [57].

We aimed to address the above gaps by using the main urban area of Shenyang as a case study and selecting various indicators from different dimensions to explore the effects of urban 2-D and 3-D morphologies on seasonal LST and their gradient effects. This study focused on the following:

1) quantitative characterization of urban morphology by selecting indicators from 2-D and 3-D perspectives;
2) investigation of the spatial pattern of seasonal LST;
3) exploitation of the XGBoost model to establish relationships and quantify the impacts of the relevant indicators on LST;
4) exploring the gradient effects of urban morphology on LST.

## II. Study Area and Data Sources

### A. Study Area

Shenyang, the capital of Liaoning Province, is positioned between 41°48'11.75" north latitude and 123°25'31.18" east longitude. It has a humid continental climate. In 2019, the lowest temperature in Shenyang during the winter was –25°C, whereas the highest temperature in the summer reached 35°C, demonstrating significant annual temperature variations. According to the Statistical Yearbook of Shenyang, the population of Shenyang reached 8.32 million by the end of 2019, with 6.74 million residing in urban areas and nearly four million living in central urban areas. Due to population concentration at the 2-D level, Shenyang has witnessed a continuous concentric expansion from its central urban region, resulting in an increase in built-up area of 357 square kilometers between 2004 and 2020. [58], [59]. At the 3-D level, according to the annual report in Shenyang, high-rise buildings are mainly concentrated in the Heping and Shenhe districts. In contrast, the concentrations of high-rise buildings in the Hunnan, Dadong, Huanggu, and Tiexi districts are noticeably lower. Hence, the distinct seasons and urban morphology made this area a good setting for your study. The main urban areas of Shenyang, including the Heping, Shenhe, Dadong, Huanggu, Tiexi, Sujiatun, Hunnan, Shenbei, and Yuhong districts, were selected for this study, as shown in Fig. 1.

### B. Data Sources

This study included multiple data sources. NPP_VIIRS was developed and produced by the Earth Observation Group (EOG) to monitor the remote sensing data of nighttime lights on the Earth's surface. NPP_VIIRS data were used to extract the city's built-up area data, determine the city centroid and development direction, and delineate urban gradients [60], [61]. Landsat 8 satellite imagery was employed to calculate the NDVI and NDBI and retrieve the LST. Land-use data were used to compute the PCL, PWG, and landscape patterns [62]. Building data were obtained from Baidu Maps to extract information such as building height, building density, and floor area ratio and were combined with DEM data to calculate the sky view factor (SVF). Population and average tree height data were obtained from WorldPop and GLAD laboratories, respectively [63], [64]. The specific data and sources are summarized in Table I.

## III. Methodology

Our methodology was comprised of the following five steps.

1) Calculation of seasonal LST in Shenyang.
2) Selection of relevant 2-D/3-D urban morphology indicators and assessment of their correlations.
3) Built-up area extraction, city centroid determination, development direction identification, and urban development gradient establishment.
4) Verification of correlations between indicators and LST.

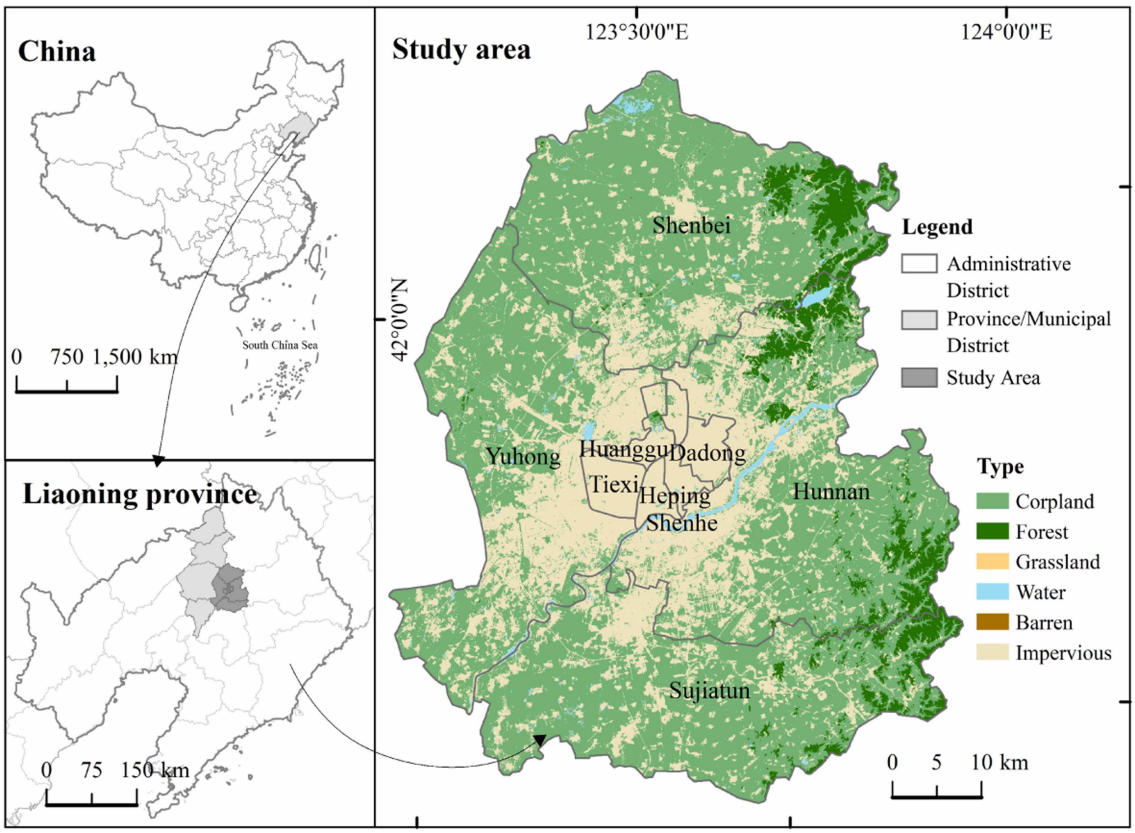


Fig. 1. Location of the study area in China.

TABLE I
DATA SOURCE AND DESCRIPTION

| Data type | Time | Spatial resolution | Source |
|---|---|---|---|
| **Administrative division** | 2019 | – | National Geomatics Center of China ( http://xzqh.mca.gov.cn/map ) |
| **Landsat8 OLI_TIRS** | 01/09 04/15 07/04 10/08 (2019) | 30m | USGS ( https://earthexplorer.usgs.gov/ ) |
| **NPP_VIIRS** | 2019 | 500m | NOAA ( https://eogdata.mines.edu/products/vnl/ ) |
| **DEM** | 2019 | 30m | Geospatial Data Cloud ( https://www.gscloud.cn ) |
| **Building data** | 12/31 (2019) | – | Baidu Maps ( https://lbsyun.baidu.com/ ) |
| **Land use** | 2019 | 30m | CLCD ( https://doi.org/10.5281/zenodo.5816591 ) |
| **Population** | 2019 | 100m | WorldPop (https://hub.worldpop.org/ ) |
| **Forest height** | 2019 | 30m | Global Forest Canopy Height ( https://glad.umd.edu/ ) |

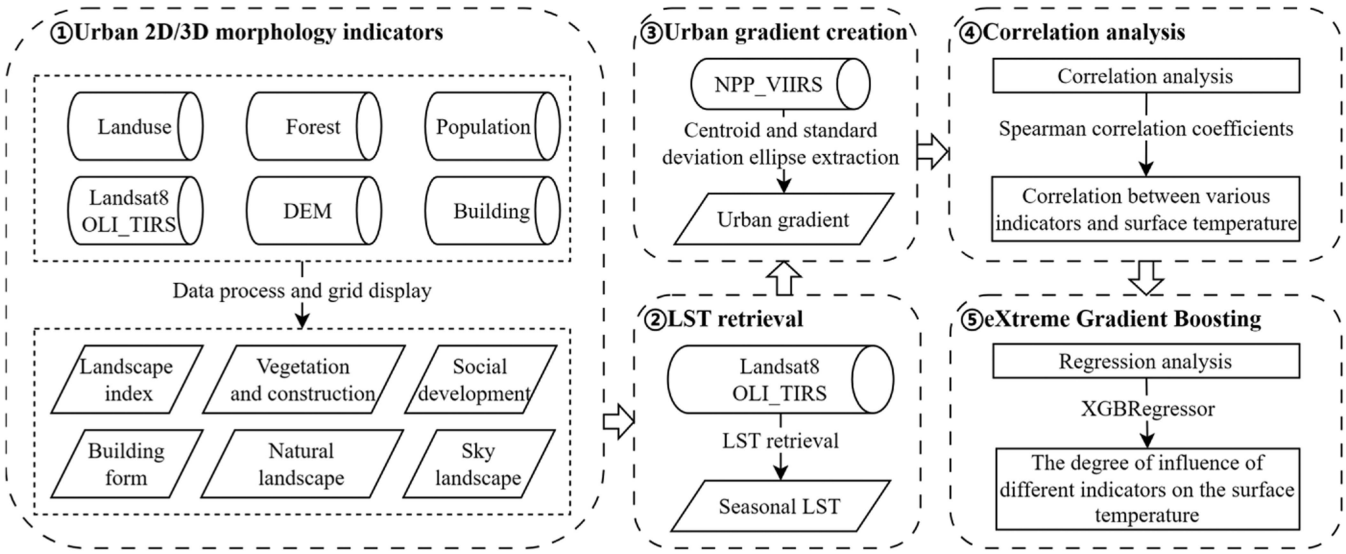


Fig. 2. Workflow of this study.

5) Utilization of XGBoost to examine the influence of different urban 2-D/3-D indicators on LST within gradients. The research workflow is illustrated in Fig. 2.

### A. LST Retrieval

There are three main methods for retrieving LST: 1) the radiative transfer equation method; 2) single-channel algorithm; and 3) split-window algorithm [65], [66], [67]. Qin et al. [68] developed a simple and highly accurate single-channel algorithm based on a radiative transfer equation.

In Planck's formula, the digital number (*DN*) value is converted to radiation intensity ($L\lambda$), and the corresponding radiation brightness *Ta* is obtained. The formula is as follows:

$$\mathrm{L}\lambda = \mathrm{Gain} \times \mathrm{DN} + \mathrm{Offse} \tag{1}$$

$$\mathrm{Ta} = \frac{K2}{ln(1+\frac{K1}{L\lambda})} \tag{2}$$

where $L\lambda$ represents the radiance intensity value, *Ta* represents the radiance brightness value, *Gain* and *Offse* represent the gain and offset parameters, which can be obtained from the Landsat header file, *DN* represents the grayscale value of the thermal infrared band, K1 = 774.89 mW/(cm$^2$ · sr · $\mu$m), K2 = 1321.08 K.

The calculation formula for LST is as follows:

$$\mathrm{Ts} = \frac{(a(1-C-D)+Ta(b(1-C-D)+C+D)-DTb}{C} - 273.15 \tag{3}$$

$$\mathrm{C} = \varepsilon\tau \tag{4}$$

$$\mathrm{D} = (1-\tau)[1+(1-)\tau] \tag{5}$$

where *Ts* represents the LST, *Ta* represents the average atmospheric temperature (*K*), *Tb* represents the brightness temperature (K), $a = -67.355351$, $b = 0.458606$, $\varepsilon$ represents the surface emissivity, and $\tau$ represents the atmospheric transmittance in the thermal infrared band. The intermediate variables C and D were also calculated.

### B. Urban 2-D/3-D Morphology Indicators

Previous studies selected indicators such as PCL and PWG to examine the relationship between urban morphology and LST. Other indicators explored include landscape patterns, building forms, and social economy [46], [33]. We performed LASSO regression to ensure the accuracy of indicator selection in 2-D/3-D urban morphology, which screened for factors more closely related to LST. After screening, variance inflation factor (VIF) computation ensured all VIF values were below 10, and there were 14 final remaining 2-D/3-D indicators divided into six categories. The 2-D indicators included landscape patterns (patch density, Shannon's diversity index, and contagion index), vegetation and construction (NDVI, NDBI, PCL, and PWG), and socioeconomic development (population). The 3-D indicators included building form (building height, building density, and floor area ratio), natural landscape (digital elevation model and mean forest height), and skyscape (sky view factor). Specific information on the indicators is provided in Table II.

All data underwent standard preprocessing, including projection and cropping. Specific enhancements included merging gridlines in building data, denoising nighttime lighting data, refining population data with annual census figures, and incorporating DEM height into the SVF calculation for improved accuracy. All indicators were uniformly aggregated into a 30×30 m grid. Notably, after the adjustment of demographic data resolution, a secondary refinement was conducted using census data to ensure precision. Finally, data normalization facilitated meaningful comparisons. Previous studies typically require that all values be greater than zero; however, this article preserved zero values that hold significance while eliminating nonsensical zero values from certain indices such as LST, PD, SHDI, CONTAG, DEM, and SVF. Landscape pattern indices underwent

TABLE II
2-D/3-D URBAN FORM INDICATORS AND DESCRIPTION

| Type | Variables | Indicators and Abbr. | Description | Unit |
|---|---|---|---|---|
| **2-D** | Landscape pattern | Patch density (PD) | Varied landscape patch densities within the grid. | #/100ha |
| | | Shannon's diversity index (SHDI) | The ratio of each patch type is multiplied by the sum of each ratio across all patch types in the grid. | / |
| | | Contagion index (CONTAG) | The degree of aggregation or expansion of each patch type in the landscape in the grid. | % |
| | Vegetation and construction | Normalized difference vegetation index (NDVI) | Average of NDVI in the grid. | / |
| | | Normalized difference built-up index (NDBI) | Average of NDBI in the grid. | / |
| | | Proportion of construction land (PCL) | Proportion of construction land area in the grid. | % |
| | | Proportion of woodland and grass (PWG) | Proportion of forest land and grassland area in the grid (%). | % |
| | Social development | Population (POP) | Population in the grid. | / |
| **3-D** | Building form | Building height (BH) | Average building height in the grid. | m |
| | | Building density (BD) | Ratio of building base area to grid area. | % |
| | | Floor area ratio (FAR) | Ratio of total building area to the grid area. | % |
| | Natural landscape | Digital elevation model (DEM) | Average of the DEM in the grid | m |
| | | Mean forest height (FOR) | The average height of the forest in the grid | m |
| | Skyscape | SVF | Average sky view factor in grid | / |

/ This unit is a dimensionless value and # represents quantity.

analysis via the Fragstats 4 platform, SVF was analyzed using the Saga platform [69], and the remaining operations were conducted using ArcGIS.

### C. Urban Gradient Creation

The utilization of nighttime light data for urban built-up area extraction is widely employed, with NPP_VIIRS data possessing superior accuracy compared to DMSP-OLS data in delineating the extent of urban built-up areas [70]. Researchers have predominantly utilized thresholding, change detection, and high-resolution remote sensing imagery-assisted methodologies [71], [72]. According to the Ministry of Housing and Urban-Rural Development's 2019 data, Shenyang's built-up area spans 563 km². In this study, we used a thresholding method to calculate the brightness values of different areas in descending order. When the cumulative area reached or exceeded the built-up area, the selected region was identified as the built-up area. Subsequently, the built-up area's centroid was extracted, and a standard deviation ellipse (SDE) was established. Based on the centroid as the center point and the proportions and orientation of the semiaxes of the ellipse, a gradient ellipse with a minor axis of 2 km was constructed.

### D. Correlation Analysis

Commonly used correlation analysis techniques include the computation of Pearson, Kendall, and Spearman correlation coefficients [73], [74]. The Pearson correlation coefficient is suitable for continuous variables and assumes that the data follow a normal distribution. For ranked data, the Kendall coefficient is favored. The Spearman correlation coefficient can accommodate nonnormally distributed data and is less sensitive to outliers. Therefore, in this study, the Spearman coefficient was used to gauge correlation direction and strength. The SPSS platform was used for computation.

TABLE III
PARAMETERS OF XGBOOST

| Parameter name | Meaning | Ranges | Default | Value |
|---|---|---|---|---|
| **eta (learning_rate)** | Step size shrinkage used in to prevents overfitting. | [0,1] | 0.3 | 0.36 |
| **gamma** | Minimum loss reduction required to make a further partition on a leaf node of the tree. | [0, ∞] | 0 | 0.75 |
| **max_depth** | Maximum depth of a tree. Increasing this value will make the model more complex and more likely to overfit. | [0, ∞] | 6 | 4 |
| **min_child_weight** | Minimum sum of instance weight (hessian) needed in a child. | [0, ∞] | 1 | 7 |
| **subsample** | Subsample ratio of the training instances. | (0,1] | 1 | 1 |
| **colsample_bytree** | The subsample ratio of columns when constructing each tree. | (0,1] | 1 | 1 |
| **colsample_bylevel** | The subsample ratio of columns for each level. | (0,1] | 1 | 0.4 |
| **lambda** | L2 regularization term on weights. | [0, ∞] | 1 | 10 |
| **alpha** | L1 regularization term on weights. | [0, ∞] | 0 | 4 |
| **n_estimators** | Number of weak learners. | (0,∞] | - | 49 |
| **seed** | Random number seed. | - | - | 33 |

### *E. XGBoost Regression Analysis*

Tree boosting is a machine learning method widely employed in regression analysis, and XGBoost has shown excellent performance in various machine learning applications [52], [75]. In previous regression analyses, researchers have predominantly utilized BRT to explore the factors influencing LST [76], [77]. XGBoost offers higher performance and efficiency than BRT, especially on tabular data [78]. It provides regularization parameters to prevent overfitting and improve model robustness. XGBoost can also directly handle missing values [56], [79].

Seasonal LST served as the dependent variable, while indicators acted as independent variables. Then, XGBoost was employed to examine the influence of 2-D/3-D urban morphology on LST. The "XGBRegressor" model was selected, and parameter refinement was conducted through "GridSearchCV." Details of specific parameters are outlined in Table III.

## IV. RESULTS

### *A. Spatial Pattern of Seasonal LST*

The single-window algorithm, created by Rozenstein et al. [80], was employed here to derive Shenyang's seasonal LST, illustrated in Fig. 3. The temperature ranges were 1.98°C–46.85°C (spring), 16.85°C–46.85°C (summer), –12.12°C–45.98°C (autumn), and –30.79°C–28.07°C (winter). The LST increased significantly during summer and decreased during winter, indicating distinct seasonal variations. The temperature difference in spring exceeded 40°C, while in autumn and winter, it exceeded 58°C. The temperature difference was relatively small in summer (approximately 30°C).

In Shenyang's central urban zone, spring and winter LST in the suburbs exceeded the city center values. High-temperature zones included the Shenbei New, Yuhong, Hunnan, and Sujiatun districts, while cooler regions were situated in the Huanggu, Shenhe, Dadong, Tiexi, and Heping districts. Conversely, high temperatures were concentrated in central urban areas in summer, with suburbs displaying cooler temperatures. Hunnan District demonstrated an elevated summer LST compared to that of the other districts. There was a distinct LST distribution in autumn, with more dispersed high-temperature zones throughout the study area and cooler spots mainly in Shenbei New District and Hunnan District, characterized by forest and water body dominance.

### *B. Indicators Contribution*

This study validated the comprehensive impact of urban morphology on LST, as depicted in Fig. 4. XGBoost regression and Spearman correlation coefficients determined positive or negative effects. When the Spearman correlation shows a positive correlation, the overall contribution is a positive contribution,

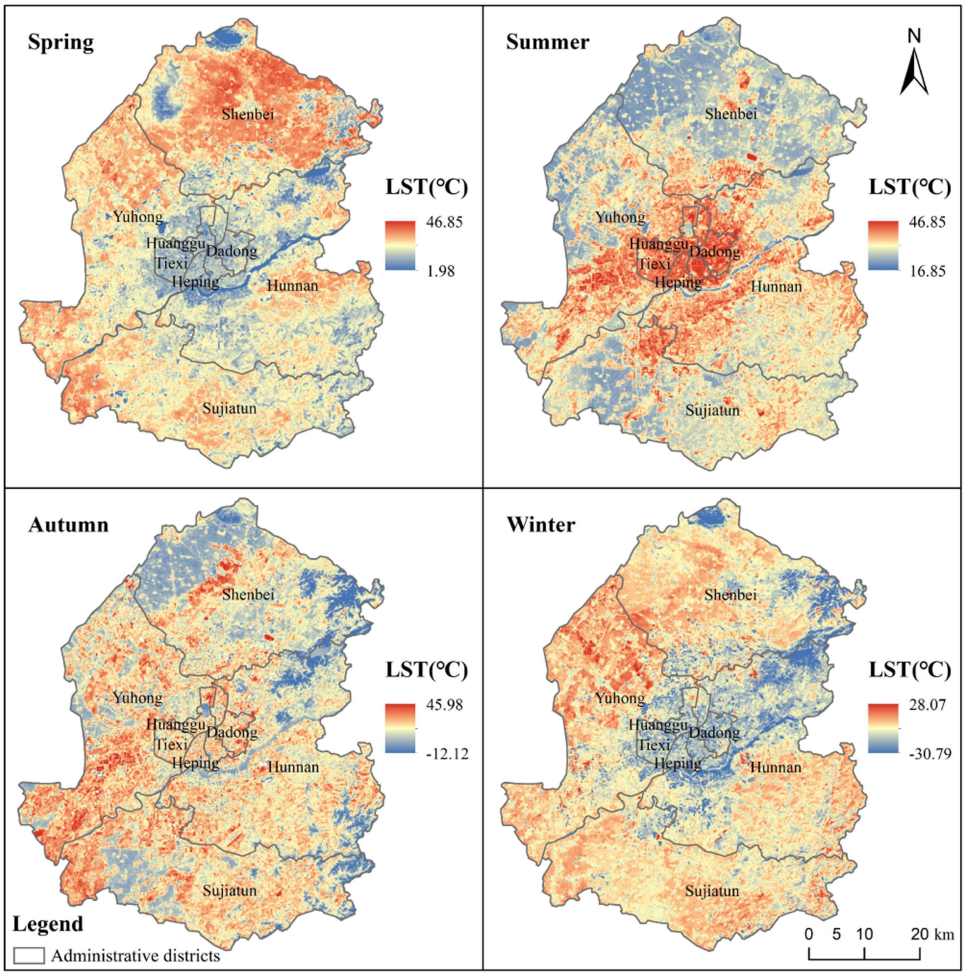


Fig. 3. Seasonal spatial pattern of LST.

and vice versa. Regarding the overall correlation between indicators and LST, all indicators displayed a significant correlation with LST at the 0.01 level. Notably, 2-D urban morphology exhibited a more substantial influence than 3-D. Vegetation and construction demonstrated the highest impact among 2-D indicators, while building form and natural landscapes wielded the greatest influence among 3-D indicators.

In spring, all indicators had a weakening effect, except for CONTAG, NDVI, and SVF, which promoted the LST. Specifically, the strongest weakening effects were observed for PCL (–0.12) and PWG (–0.38) among the 2-D indicators and FOR (–0.17) and BD (–0.09) among the 3-D indicators. The positive and negative impacts during winter were similar to those in spring; however, the overall impact was lower than that in spring, except for vegetation and construction. In summer, the trends were generally opposite those observed in spring and winter. All indicators had a promoting effect on LST, except for CONTAG, NDVI, and PWG among the 2-D indicators and FOR and SVF among the 3-D indicators. Notably, NDBI (0.42) and PCL (0.39) had the greatest effects on LST. In autumn, the impact of PWG was significantly higher than that of the other indicators (0.89), followed by FOR (0.039). Overall, NDBI consistently had a positive effect on LST, whereas PWG and FOR typically had negative effects, contributing to a reduction in LST.

### C. *Correlation Between Indicators and LST*

To examine the correlation between different indicators and LST across the gradients, we employed Spearman's correlation coefficient. The distribution of urban gradients is illustrated in Fig. 5, and the correlation results of different indicators across the gradients are presented in Fig. 6. Regarding the gradient correlation between indicators and LST, the significance level was set at 0.01 for 98% of the indicators.

In the 2-D urban morphology, the landscape pattern indices PD and SHDI showed consistent patterns. With increasing gradients, the correlations transitioned from weakly negative to positive during spring and winter. Beyond the 10 km gradient, the correlations reversed to become negative and stronger, reaching a maximum of 0.49. In summer and autumn, the correlations weakened from strongly negative (–0.57) to positive correlations between the 12 and 16 km gradients and strengthened with an increasing gradient (0.5). CONTAG exhibited a strong correlation within the 12–26 km gradient, with a predominantly positive

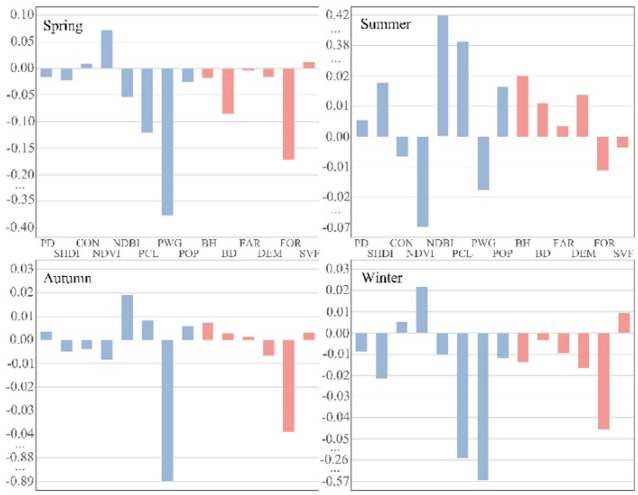


Fig. 4. Contribution of indicators to LST. From left to right and from top to bottom are spring, summer, autumn, and winter. Blue represents 2-D urban morphology, and pink represents 3-D urban morphology.

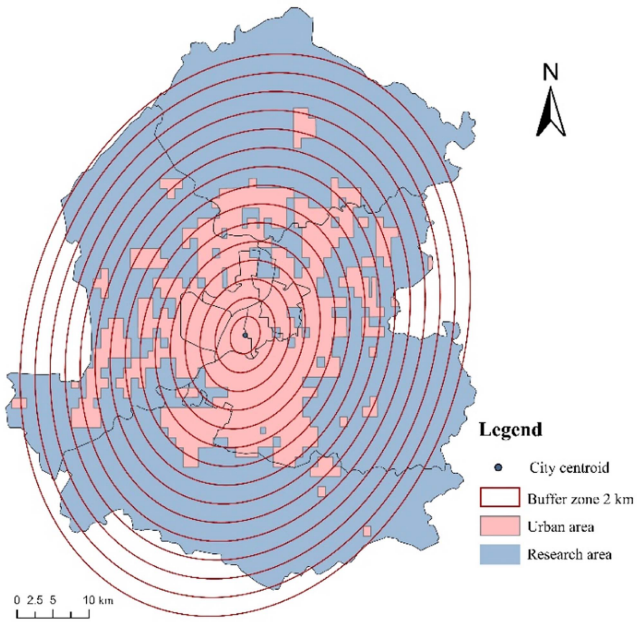


Fig. 5. Urban area and urban gradient buffer zone.

correlation during spring and winter and negative correlations during summer and autumn. NDVI and NDBI consistently showed opposite correlations among the vegetation and construction indicators, with NDVI exhibiting a positive correlation in spring and winter, and NDBI exhibiting a negative correlation. This pattern was reversed in the summer and autumn. Notably, NDVI and NDBI strongly correlated with LST in summer, reaching 0.79. PCL exhibited a negative correlation in spring and winter and a positive correlation in summer and autumn. PWG consistently showed negative correlations with LST across all seasons, with increasing strength in correlation across gradients ranging from –0.01 to –0.47. Regarding the social development indicator in the 2-D morphology, POP exhibited a pattern similar to that of PCL. This promoted LST increases during spring and winter and decreases during summer and autumn.

Regarding 3-D urban morphology, the building form indicators typically had a positive effect on LST closer to the city center, especially during summer and autumn. Even at a distance of 30 km from the center, they still stimulated an increase in LST. As the distance increased in spring, autumn, and winter, the building form indicators weakly increased the LST. Interestingly, within 14 km from the center, the BH, BD, and FAR indicators exhibited different correlations, with BD consistently having the highest correlation across all four seasons, reaching 0.49. Beyond the 14 km range, correlations between building form indicators and LST gradually decreased and became consistent, approaching zero. This was due to the decrease in the number of buildings as the distance from the center increased. Among the natural landscape indicators, DEM showed a stronger correlation with LST beyond 22 km and within 8 km from the center, with a maximum correlation of 0.61. FOR exhibited predominantly negative correlations with LST, with the correlation increasing with distance from the center during spring and winter, decreasing during summer, and showing relatively consistent correlations during autumn. This may be attributed to vegetation withering in autumn, which affects correlation strength. In terms of SVF within the skyscape indicators, the patterns were similar during spring and winter. Strong positive correlations were observed within a 4–12 km gradient. In summer, SVF exhibited a negative correlation within this range. In autumn, the correlations were relatively uniform across different gradients.

Overall, the correlations between the indicators and LST were most pronounced during the summer. Autumn exhibited similar patterns to summer but with lower correlations. Spring and winter exhibited similar patterns, except for PWG, DEM, and SVF, which demonstrated contrasting patterns to those in summer and autumn.

### *D. Gradient Effect*

Different gradients have significant variations in the impact of the indicators on LST [46]. In our study, based on the city center and development direction, 15 gradients were divided within a radius of 2 km, ranging from 0 to 30 km. As shown in Fig. 5, this study classified the gradients into three ranges: within 14 km, 14–24 km, and 24–30 km, representing urban, suburban, and fringe areas, respectively. This study explored alterations in indicator effects on LST within diverse gradients, with the findings illustrated in Fig. 7.

In the urban area within a range of 14 km, where the built-up area exceeds 50%, significant impacts were observed from landscape patterns and social development among the 2-D indicators and building form and skyscape among the 3D indicators. As the distance approached 14 km, the degree of influence gradually decreased. The landscape pattern index, SHDI, exhibited the largest variation in summer, decreasing from 0.49 to 0.02. A higher LST is often observed in the city center during summer, and increasing the fragmentation of landscapes and enhancing land-use diversity can effectively reduce the LST. Among the

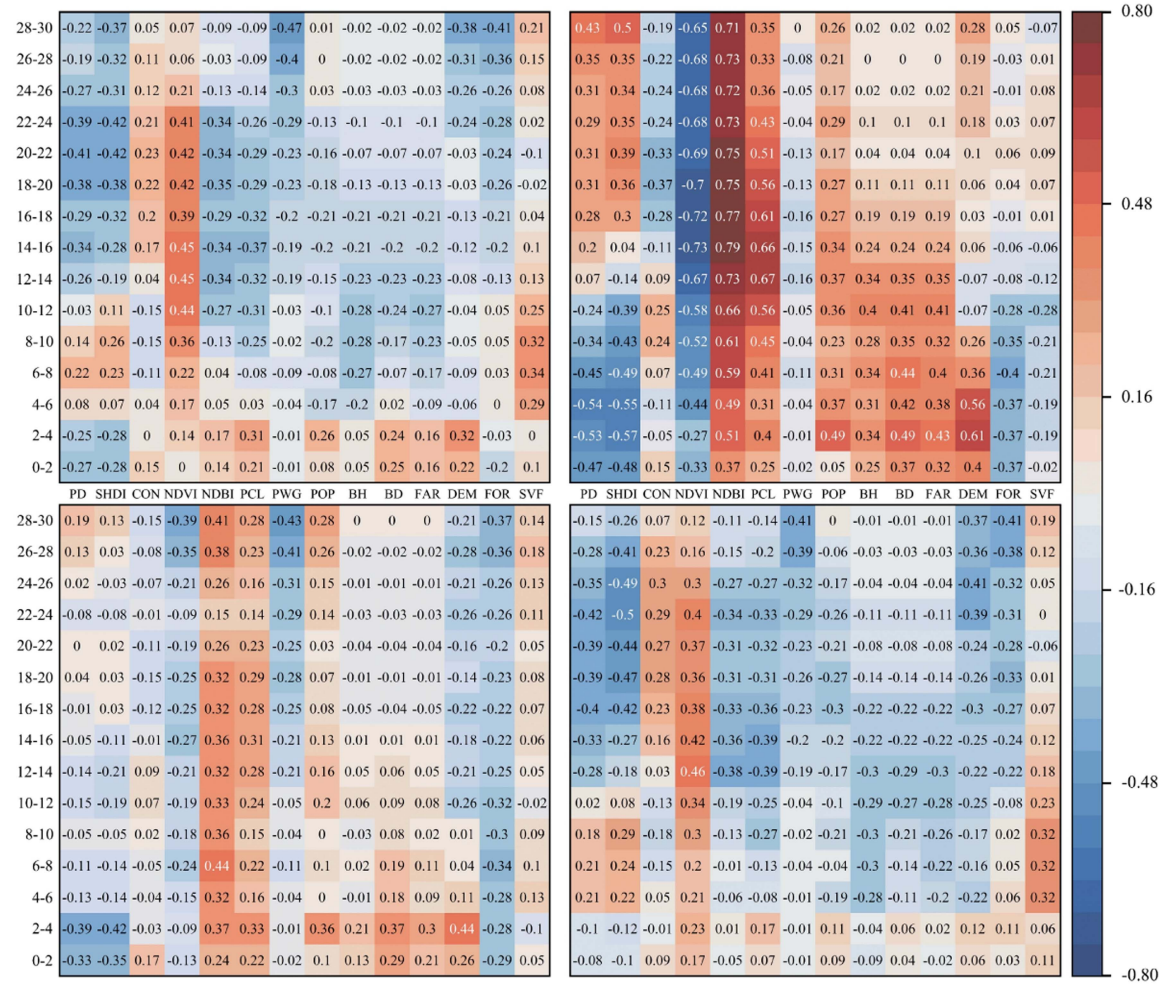


Fig. 6. Correlation between urban form and LST. From left to right and from top to bottom are spring, summer, autumn, and winter.

vegetation and construction indicators, NDVI and NDBI also showed a high influence in all seasons other than summer, which showed the opposite pattern, where their impact within the 14-km range was lower. The influence of the DEM within the urban area was also relatively high but decreased with increasing distance, similar to the FOR.

In suburban areas ranging from 14 to 24 km, where the built-up area exceeds 10% but is less than or equal to 50%, the influence of landscape patterns on the 2-D indicators remained relatively low. Within the vegetation and construction indicators, PCL and PWG reached peak influence, with PCL exhibiting a maximum impact (0.62) in summer and PWG reaching 0.92 in autumn. The influences of NDBI and NDVI also increased along the suburban gradient during summer. Among the 3-D indicators, the influence of building form was lower compared to that of the urban area but still had some impact, with BH reaching a maximum influence of 0.14. However, as the distance increased towards the edge of the area, the degree of influence continued to decrease. Within the natural landscape, FOR exerted a stronger influence in the suburban area due to elevated tree count compared to that of urban areas. The influence of DEM also showed an upward trend. The skyscape exhibited a similar pattern to the building form, with a decreasing degree of influence; however, the decline in the impact of skyscapes was higher than that of the building form indicators.

In the fringe area (beyond 24 km, where the built-up area is less than or equal to 10%), the influence of PWG among the 2-D indicators, the impact of NDBI and NDVI during the summer season, and the influence of natural landscape on the 3D indicators were evident. Artificial surfaces were scarce in the fringe area, and natural-related indicators, such as PWG and FOR, were more abundant in this region, leading to a higher degree of influence on LST. Human activities were less pronounced in this area than in suburban areas, resulting in a higher degree of influence. Additionally, because of the minimal building presence in the fringe area, the impact of the building forms tended toward zero.

Generally, the landscape pattern within the 2-D morphology and the building form and skyscape within the 3-D morphology exhibited unimodal patterns exhibited peak values concentrated in urban areas. Social development within the 2-D morphology and natural landscape within the 3-D morphology showed a bimodal pattern, with peaks concentrated in both urban and fringe areas. NDBI, NDVI, and PCL exhibited unimodal

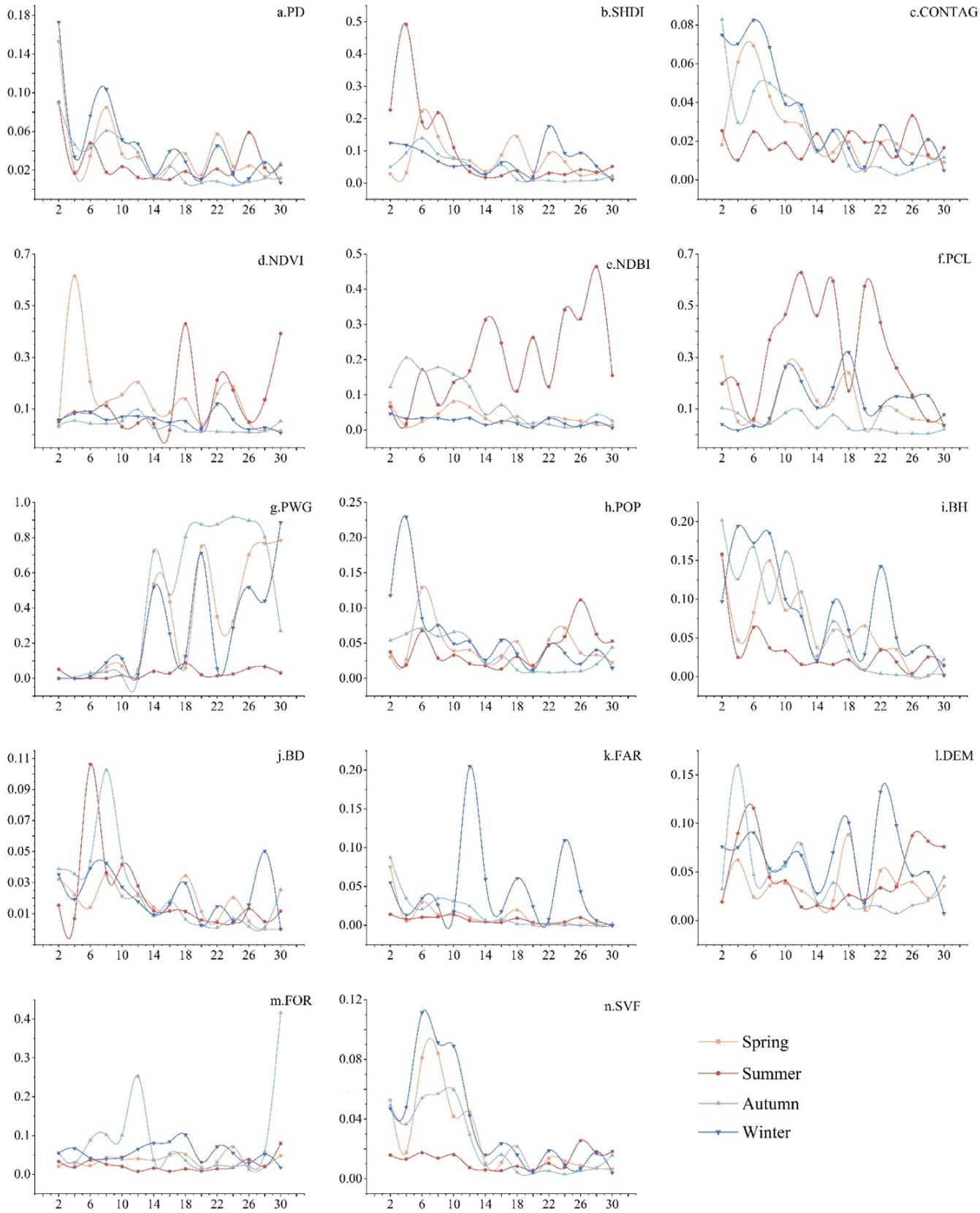


Fig. 7. Gradient effect of each index in different seasons.

TABLE IV
$R^2$ AND MSE OF XGBOOST MODEL UNDER VARIOUS GRADIENTS IN FOUR SEASONS

| Gradient (km) | R2 | | | | MSE | | | |
|---|---|---|---|---|---|---|---|---|
| **Season** | **Spring** | **Summer** | **Autumn** | **Winter** | **Spring** | **Summer** | **Autumn** | **Winter** |
| **0–2** | 0.64 | 0.84 | 0.6 | 0.51 | 8.04* | 4.17*** | 1.64** | 1.26** |
| **2–4** | 0.9 | 0.93 | 0.72 | 0.3 | 8.72* | 1.09** | 1.16** | 2.06** |
| **4–6** | 0.84 | 0.87 | 0.75 | 0.63 | 8.77* | 1.22** | 1.04** | 1.30** |
| **6–8** | 0.82 | 0.84 | 0.67 | 0.6 | 9.65* | 1.35** | 1.43** | 1.33** |
| **8–10** | 0.77 | 0.81 | 0.62 | 0.55 | 1.13** | 1.49** | 1.38** | 1.61** |
| **10–12** | 0.78 | 0.83 | 0.69 | 0.59 | 1.29** | 1.45** | 1.08** | 1.27** |
| **12–14** | 0.77 | 0.83 | 0.72 | 0.67 | 1.36** | 1.63** | 1.25** | 1.24** |
| **14–16** | 0.77 | 0.85 | 0.69 | 0.68 | 1.18** | 1.50** | 1.24** | 1.16** |
| **16–18** | 0.76 | 0.83 | 0.71 | 0.73 | 1.46** | 1.55** | 1.35** | 9.25* |
| **18–20** | 0.76 | 0.84 | 0.7 | 0.7 | 1.43** | 1.36** | 1.42** | 8.83* |
| **20–22** | 0.82 | 0.84 | 0.66 | 0.73 | 1.35** | 1.34** | 1.47** | 7.83* |
| **22–24** | 0.79 | 0.84 | 0.61 | 0.77 | 1.72** | 1.31** | 1.79** | 8.08* |
| **24–26** | 0.68 | 0.83 | 0.65 | 0.73 | 2.21** | 1.36** | 1.79** | 7.21* |
| **26–28** | 0.63 | 0.84 | 0.72 | 0.64 | 2.70** | 1.46** | 1.62** | 1.01** |
| **28–30** | 0.7 | 0.86 | 0.73 | 0.62 | 2.44** | 1.24** | 1.67** | 1.28** |

* represents E-06; ** represents E-05,and *** represents E-03.

patterns except for in summer, with the former two concentrated in urban areas and the latter concentrated in suburban areas. PWG demonstrated a bimodal pattern, with higher influences in the suburban and fringe areas. In summer, NDBI, NDVI, and PWG showed bimodal patterns, with peaks concentrated in the suburban and fringe areas, whereas PCL exhibited a unimodal pattern in the suburban area. Table IV presents the coefficients of determination ($R^2$) and mean square error (MSE) for each gradient and seasonal LST. Summer exhibited the highest R2 value, with consistently low MSE values across gradients, confirming strong model reliability.

## V. DISCUSSION

### A. *Effects of 2-D/3-D Indexes on Seasonal LST*

Prior research predominantly concentrated on the impact of urban morphology on LST within single seasons. This study addresses this gap by examining Shenyang's distinct seasons, enhancing the available literature. From the perspective of different seasons, there was a higher similarity between spring and winter, whereas summer and autumn exhibited some similarities, aligning with the findings of Chen et al. [33], [52] Scholars have noted that the surface temperature of snow-climate cities in China exhibits a marked seasonality, with dominant factors varying significantly between seasons [81]. Some researchers categorize spring and autumn together as transitional seasons [82]. When transitioning to summer or winter, a substantial influence from the preceding season is retained. For example, during the transitional season of spring, the melting snow generates water that is absorbed by the soil, and it has been proven that water can effectively reduce LST [83]. Therefore, as the gradient increases, the expansion of nonartificial surfaces enhances the land's capacity to absorb water, which in turn strengthens the correlation between indices such as PD, SHDI, PWG, and FOR [84], [85]. During summer and autumn, the heat island effect predominates, and the heat absorption capacity of artificial surfaces intensifies [22].

Consequently, indices like PCL, NDBI, BH, and BD exhibit a positive correlation with LST, as opposed to that observed during winter and spring, with the NDBI showing the strongest correlation, in alignment with the results of Peng et al. [82]. Notably, the regression analysis for summer presents a more accurate fit compared to the other three seasons. Several factors may account for this: First, the climate in summer is more stable in snow-climate cities in China, with less fluctuation in sunny day environmental variables and lower cloud quantities in remote sensing images, resulting in more accurate retrieval of LST. Summer, unlike other seasons, features a greater diversity

and activity of indicators, aiding the model in capturing the impacts of various indicators on LST. The heat island effect results in higher temperatures in central urban areas compared to the suburbs and the urban fringe, accentuating the thermal contrast between the inner and outer city areas, which leads to more effective regression modeling.

In terms of the selected indicators and their impact levels, this study considered 14 indicators from both 2-D and 3-D urban morphologies, covering various aspects such as landscape, vegetation, construction, and buildings. This comprehensive approach rectifies the research gap concerning the impacts of the natural landscape on LST [36], [86]. The crux of our methodology involved a meticulous screening of selected indicators, which were classified into two main categories and six subcategories. Significance was attributed to the zero values of numerous indicators to justify their inclusion, such as BH, BD, and FAR, which, at zero, indicate a lack of buildings, thereby allowing other indicators to take precedence within the region. Conversely, zero values for indicators such as landscape pattern indexes, DEM, and SVF were systematically eliminated from consideration. This operation also greatly improved the R2 calculated by the model and greatly reduced the MSE value.

Among the 2-D morphological indicators, vegetation and construction significantly influenced LST, aligning with the results of Guo et al. [46]. Artificial construction tends to absorb more solar radiation and store heat, resulting in increased LST. Conversely, the transpiration process of vegetation acts as a cooling system, leading to a decrease in LST. Therefore, the FOR in the 3-D index weakens the LST [87]. Within the landscape pattern, the SHDI had a higher impact on LST than PD and CONTAG, indicating that increasing land-use diversity and balance within patches is favorable for cooling the land surface. Among the 3-D indicators, the building form was also identified as an important factor influencing LST. Yang et al. [88] found that BD had the most significant impact on LST, whereas Chen et al. [33], [52], [84] highlighted BH as the most important factor. However, this study found that BD had a higher impact in spring than BH, whereas BH had a greater influence during summer, autumn, and winter. This difference may be attributed to seasonal variation. SVF, on the other hand, was observed to lower LST in summer while providing a warming effect in other seasons.

### B. Gradient Change in 2-D/3-D Index Contribution

Prior research into the urban morphology-LST gradient predominantly centered on the urban–rural distinction, neglecting continuous variations within this spectrum [89], [90]. In this study, the center of urban development was identified, and 15 gradients were delineated, creating a coherent connection within the main urban area of Shenyang. This allowed us to investigate how urban morphology indicators varied with distance from the city center. Concentric circular gradients were not adopted in this study to better align them with urban development. Instead, an SDE was chosen as the basis for proportional delineation, capturing the primary contours and dominant directions of the spatial distribution. Standard deviation ellipses provide good visual and effective representations of regional spatial patterns [91], [92].

Researchers typically employ regression models to validate the correlation between indicators and LST. Machine learning methods, such as RF, have also been utilized to quantify the impact of indicators. However, these quantifications are primarily expressed in absolute terms and cannot demonstrate the positive or negative nature of these effects. In this study, we employed XGBoost to calculate the impacts of different indicators and combined them with Spearman's correlation coefficients to validate the directionality of their influences on LST.

We found that the impacts of landscape patterns and social development on 2-D morphology and building form and skyscape on 3-D morphology on the LST decreased with distance. Conversely, vegetation-related indicators, such as PWG and FOR, exhibited the opposite trend, with higher impacts observed further from the city center. These findings align with those of Liang et al. [37], [44] and Zhang et al. [33], [52], [84]. As urbanization expands outward from the city center, building numbers and heights gradually diminish, reducing their LST impact. Moving away from the center, heightened vegetation coverage and decreased artificial surroundings have a greater LST influence [93], [90].

### C. XGBoost Model Selection

In selecting the model, we focused on two main factors: first, the treatment of zero values in the data. As discussed in Section V, Section B, the retention or exclusion of zero values for different indicators is critical; XGBoost excels at managing such data, which has significantly improved the model's $R^2$ and substantially reduced the MSE. Second, the selection was due to XGBoost's computational efficiency and fitting performance. Despite other mainstream methods exhibiting high effectiveness, XGBoost outperformed them in our study, which involved complex and large datasets.

Compared to BRT, both of which are machine learning methods based on Boosted Trees algorithms, XGBoost has shortened computation times and can handle larger datasets due to algorithmic enhancements and systemic improvements. Against RF, another supervised learning algorithm, XGBoost typically achieves greater precision, particularly with extensive engineering datasets. With millions of records in our dataset, XGBoost provided superior processing speed and predictive accuracy over RF. We conduct our experiments with an Intel(R) Xeon(R) W-2223 CPU @ 3.60GHz CPU, and under the same experimental conditions, the processing times for three methods when handling a dataset containing 172 186 records were as follows: XGBoost (3.92 s) $>$ BRT (12.00 s) $>$ RF (28.41 s). To further ascertain XGBoost's performance, we selected 15 gradients in the summer with the best performance as experimental samples, and Table V shows the results of the experiment. The results, presented in Table V, affirmed XGBoost's superior efficacy.

### D. Implications for Urban Planning

Studies indicate that both 2-D and 3-D urban morphologies exert substantial influence on LST. Strategic urban morphology planning can effectively mitigate LST and achieve a healthier living environment. Urban planners can exercise control over building height and density in areas closer to city centers to

TABLE V
$R^2$ AND MSE VALUES OF XGBOOST, BRT, AND RF

| | | 0-2 | 2–4 | 4–6 | 6–8 | 8–10 | 10–12 | 12–14 | 14–16 | 16–18 | 18–20 | 20–22 | 22–24 | 24–26 | 26–28 | 28–30 |
|---|---|---|---|---|---|---|---|---|---|---|---|---|---|---|---|---|
| $R^2$ | XGB | 0.84 | 0.93 | 0.87 | 0.84 | 0.81 | 0.83 | 0.83 | 0.85 | 0.83 | 0.84 | 0.84 | 0.84 | 0.83 | 0.84 | 0.86 |
| | BRT | 0.79 | 0.91 | 0.84 | 0.78 | 0.75 | 0.76 | 0.79 | 0.8 | 0.8 | 0.79 | 0.8 | 0.79 | 0.78 | 0.8 | 0.83 |
| | RF | 0.72 | 0.9 | 0.8 | 0.74 | 0.7 | 0.73 | 0.75 | 0.78 | 0.77 | 0.76 | 0.75 | 0.75 | 0.72 | 0.76 | 0.8 |
| MSE | XGB | 4.17 ** | 1.09 * | 1.22 * | 1.35 * | 1.49 * | 1.45 * | 1.63 * | 1.50 * | 1.55 * | 1.36 * | 1.34 * | 1.31 * | 1.36 * | 1.46 * | 1.24 * |
| | BRT | 5.60 ** | 1.39 * | 1.51 * | 1.85 * | 1.98 * | 1.97 * | 2.08 * | 2.02 * | 1.82 * | 1.81 * | 1.73 * | 1.69 * | 1.78 * | 1.79 * | 1.60 * |
| | RF | 7.57 ** | 1.67 * | 1.88 * | 2.22 * | 2.36 * | 2.27 * | 2.50 * | 2.27 * | 2.15 * | 2.12 * | 2.10 * | 2.08 * | 2.21 * | 2.17 * | 1.88 * |

* represents E-05; ** represents E-03.

minimize the warming effect of building forms on LST. They can also balance the distribution of landscapes within urban areas by incorporating more vegetation- and landscape-related features into central urban zones. These measures can reduce the LST. Furthermore, increasing the number of trees can alleviate the heat-promoting effects of buildings in central urban areas.

### *E. Limitations*

This study examined the impact of urban 2-D/3-D indicators on LST across diverse seasons and gradients, addressing a prior research gap. Nonetheless, certain limitations of this study warrant acknowledgment. First, the resolutions of the selected indicators were inconsistent. Although the population data were adjusted to ensure accuracy to the greatest extent possible, further improvements are needed compared to data with higher resolutions. Second, this study examined only four seasons in one year without considering interannual variations. A time-series analysis could yield more precise insights into indicator influences on LST. Third, obtaining complete seasonal remote sensing images for many cities, especially those with lower latitudes, is challenging due to cloud cover and access limitations. In the future, scholars can utilize more data or alternative approaches to assess and analyze the LSTs of other cities. Fourth, this study employed standard deviation ellipses to define urban gradients, which better reflect the city's center and development direction. However, different cities may require different gradient divisions based on their unique development patterns, such as urban road networks.

## VI. CONCLUSION

This study employed XGBoost to explore the positive and negative impacts of 2-D and 3-D urban morphologies on LST and their gradient effects. The conclusions are as follows.

1) There were significant differences in the LST across the four seasons in Shenyang. During spring and winter, the suburban areas exhibited a higher LST than the city center, primarily concentrated in the Shenbei, Yu Hong, Hunnan, and Sujiatun districts. In contrast, during summer, the city center experienced a higher LST, concentrated in the Huanggu, Shenhe, Dadong, Tiexi, and Heping districts. The LST distribution in autumn was scattered and uniform.
2) According to the Spearman correlation calculation, all indices in summer had strong correlations with LST, showing the same regularity in summer and autumn and the same regularity in spring and winter. Except for PWG, DEM, and SVF, all indices showed opposing patterns compared with those in summer and autumn.
3) Among the various indicators, the 2-D urban morphology indicators of vegetation and construction exerted the greatest influence on the LST, with PWG having the highest impact in autumn (up to 0.89). The next most influential factors were the BD of 3-D urban morphology indicators and the FOR of natural landscapes.
4) We observed significant differences in the impacts of different indicators across various gradients. In urban areas, landscape patterns, social development, building forms, natural landscapes, and skyscapes had the greatest influence. In suburban areas, vegetation and construction indicators had a notable impact, and building forms exhibited a certain influence. In the fringe areas, vegetation and construction, social development, and natural landscape indicators demonstrated a relatively high influence.

In summary, our results highlight the influence of 2-D and 3-D urban morphologies on LST, providing valuable insights into planning strategies to create cooler cities and promote sustainable urban development.

## REFERENCES


[1] L. J. C. Ma, "Urban Transformation in China, 1949 –2000: A review and research agenda," *Environ Plan A*, vol. 34, no. 9, pp. 1545–1569, Sep. 2002, doi: 10.1068/a34192.

[2] J. van Vliet, "Direct and indirect loss of natural area from urban expansion," *Nat Sustain*, vol. 2, no. 8, Aug. 2019, Art. no. 8, doi: 10.1038/s41893-019-0340-0.

[3] A.-L. Balogun et al., "Assessing the potentials of digitalization as a tool for climate change adaptation and sustainable development in urban centres," *Sustain. Cities Soc.*, vol. 53, Feb. 2020, Art. no. 101888, doi: 10.1016/j.scs.2019.101888.

[4] I. Khan, F. Hou, and H. P. Le, "The impact of natural resources, energy consumption, and population growth on environmental quality: Fresh evidence from the United States of America," *Sci. Total Environ.*, vol. 754, Feb. 2021, Art. no. 142222, doi: 10.1016/j.scitotenv.2020.142222.

[5] W. Yu et al., "Downscaling mapping method for local climate zones from the perspective of deep learning," *Urban Climate*, vol. 49, May 2023, Art. no. 101500, doi: 10.1016/j.uclim.2023.101500.

[6] J. Qin, C. Fang, Y. Wang, G. Li, and S. Wang, "Evaluation of three-dimensional urban expansion: A case study of Yangzhou City, Jiangsu Province, China," *Chin. Geogr. Sci.*, vol. 25, no. 2, pp. 224–236, Apr. 2015, doi: 10.1007/s11769-014-0728-8.

[7] H. Dadashpoor, P. Azizi, and M. Moghadasi, "Land use change, urbanization, and change in landscape pattern in a metropolitan area," *Sci. Total Environ.*, vol. 655, pp. 707–719, Mar. 2019, doi: 10.1016/j.scitotenv.2018.11.267.

[8] S. C. Valencia et al., "Adapting the Sustainable Development Goals and the New Urban Agenda to the city level: Initial reflections from a comparative research project," *Int. J. Urban Sustain. Develop.*, vol. 11, no. 1, pp. 4–23, Jan. 2019, doi: 10.1080/19463138.2019.1573172.

[9] Y. Li, X. Kong, and Z. Zhu, "Multiscale analysis of the correlation patterns between the urban population and construction land in China," *Sustain. Cities Soc.*, vol. 61, Oct. 2020, Art. no. 102326, doi: 10.1016/j.scs.2020.102326.

[10] X. Cai, J. Yang, Y. Zhang, X. Xiao, and J. (Cecilia) Xia, "Cooling island effect in urban parks from the perspective of internal park landscape," *Humanit Soc Sci Commun*, vol. 10, no. 1, Oct. 2023, Art. no. 1, doi: 10.1057/s41599-023-02209-5.

[11] T. R. Oke, "City size and the urban heat island," *Atmospheric Environ. (1967)*, vol. 7, no. 8, pp. 769–779, Aug. 1973, doi: 10.1016/0004-6981(73)90140-6.

[12] H. Su, G. Han, L. Li, and H. Qin, "The impact of macro-scale urban form on land surface temperature: An empirical study based on climate zone, urban size and industrial structure in China," *Sustain. Cities Soc.*, vol. 74, Nov. 2021, Art. no. 103217, doi: 10.1016/j.scs.2021.103217.

[13] R. Zhang, J. Yang, X. Ma, X. Xiao, and J. (Cecilia) Xia, "Optimal allocation of local climate zones based on heat vulnerability perspective," *Sustain. Cities Soc.*, vol. 99, Dec. 2023, Art. no. 104981, doi: 10.1016/j.scs.2023.104981.

[14] J. Ren, J. Yang, F. Wu, W. Sun, X. Xiao, and J. (Cecilia) Xia, "Regional thermal environment changes: Integration of satellite data and land use/land cover," *iScience*, vol. 26, no. 2, Feb. 2023, Art. no. 105820, doi: 10.1016/j.isci.2022.105820.

[15] J. W. Baldwin, J. B. Dessy, G. A. Vecchi, and M. Oppenheimer, "Temporally compound heat wave events and global warming: An emerging hazard," *Earth's Future*, vol. 7, no. 4, pp. 411–427, 2019, doi: 10.1029/2018EF000989.

[16] F. R. Siegel, *Adaptations of Coastal Cities to Global Warming, Sea Level Rise, Climate Change and Endemic Hazards*. Springer, 2019.

[17] R. Zhang et al., "Warming and cooling effects of local climate zones on urban thermal environment," *Front. Public Health*, vol. 10, Nov. 2022, Art. no. 1072174, doi: 10.3389/fpubh.2022.1072174.

[18] X. Ma, J. Yang, D. Sun, R. Zhang, X. Xiao, and J. Xia, "Fine allocation of sectoral carbon emissions at block scale and contribution of functional zones," *Ecological Inform.*, vol. 78, Dec. 2023, Art. no. 102293, doi: 10.1016/j.ecoinf.2023.102293.

[19] Q. Shen et al., "StreetVizor: Visual exploration of Human-scale urban forms based on street views," *IEEE Trans. Visual. Comput. Graph.*, vol. 24, no. 1, pp. 1004–1013, Jan. 2018, doi: 10.1109/TVCG.2017.2744159.

[20] J. Yang, J. Su, J. Xia, C. Jin, X. Li, and Q. Ge, "The impact of spatial form of urban architecture on the Urban thermal environment: A case study of the Zhongshan district, Dalian, China," *IEEE J. Sel. Topics Appl. Earth Observ. Remote Sens.*, vol. 11, no. 8, pp. 2709–2716, Aug. 2018, doi: 10.1109/JSTARS.2018.2808469.

[21] J.-P. Chang et al., "Assessing spatial synergy between integrated Urban rail Transit system and urban form: A BULI-based MCLSGA model with the wisdom of crowds," *IEEE Trans. Fuzzy Syst.*, vol. 31, no. 2, pp. 434–448, Feb. 2023, doi: 10.1109/TFUZZ.2022.3185680.

[22] C. Li, J. Yang, and Y. Zhang, "Evaluation and analysis of the impact of coastal urban impervious surfaces on ecological environments," *IEEE J. Sel. Topics Appl. Earth Observ. Remote Sens.*, vol. 16, pp. 8721–8733, 2023, doi: 10.1109/JSTARS.2023.3310616.

[23] Y. Xie, D. Feng, S. Xiong, J. Zhu, and Y. Liu, "Multi-scene building height estimation method based on shadow in high resolution imagery," *Remote Sens.*, vol. 13, no. 15, Art. no. 15, Jan. 2021, doi: 10.3390/rs13152862.

[24] P. Dou and Z. Han, "Quantifying land use/land cover change and urban expansion in Dongguan, China, from 1987 to 2020," *IEEE J. Sel. Topics Appl. Earth Observ. Remote Sens.*, vol. 15, pp. 201–209, 2022, doi: 10.1109/JSTARS.2021.3133703.

[25] Y. Lu, W. Yue, T. He, and Z. Shan, "Urban form centrality and thermal environment: An empirical study of Chinese megacities," *Sustain. Cities Soc.*, vol. 83, Aug. 2022, Art. no. 103955, doi: 10.1016/j.scs.2022.103955.

[26] R. Guo, H. Leng, Q. Yuan, and S. Song, "Impact of urban form on CO2 emissions under different socioeconomic factors: Evidence from 132 small and medium-sized cities in China," *Land*, vol. 11, no. 5, May 2022, Art. no. 713, doi: 10.3390/land11050713.

[27] H. Liu, B. Huang, Q. Zhan, S. Gao, R. Li, and Z. Fan, "The influence of urban form on surface urban heat island and its planning implications: Evidence from 1288 urban clusters in China," *Sustain. Cities Soc.*, vol. 71, Aug. 2021, Art. no. 102987, doi: 10.1016/j.scs.2021.102987.

[28] A. Frenkel and M. Ashkenazi, "Measuring urban sprawl: How can we deal with it?," *Environ Plann B Plann Des*, vol. 35, no. 1, pp. 56–79, Feb. 2008, doi: 10.1068/b32155.

[29] M. Harari, "Cities in bad shape: Urban geometry in India," *Amer. Econ. Rev.*, vol. 110, no. 8, pp. 2377–2421, Aug. 2020, doi: 10.1257/aer.20171673.

[30] G. Xu, Z. Zhou, L. Jiao, and R. Zhao, "Compact urban form and expansion pattern slow down the decline in urban densities: A global perspective," *Land Use Policy*, vol. 94, May 2020, Art. no. 104563, doi: 10.1016/j.landusepol.2020.104563.

[31] D. Mutiibwa, S. Strachan, and T. Albright, "Land surface temperature and surface air temperature in complex terrain," *IEEE J. Sel. Topics Appl. Earth Observ. Remote Sens.*, vol. 8, no. 10, pp. 4762–4774, Oct. 2015, doi: 10.1109/JSTARS.2015.2468594.

[32] C. Yin, M. Yuan, Y. Lu, Y. Huang, and Y. Liu, "Effects of urban form on the urban heat island effect based on spatial regression model," *Sci. Total Environ.*, vol. 634, pp. 696–704, Sep. 2018, doi: 10.1016/j.scitotenv.2018.03.350.

[33] Y. Chen, J. Yang, W. Yu, J. Ren, X. Xiao, and J. C. Xia, "Relationship between urban spatial form and seasonal land surface temperature under different grid scales," *Sustain. Cities Soc.*, vol. 89, Feb. 2023, Art. no. 104374, doi: 10.1016/j.scs.2022.104374.

[34] A. Vartholomaios, "A parametric sensitivity analysis of the influence of urban form on domestic energy consumption for heating and cooling in a Mediterranean city," *Sustain. Cities Soc.*, vol. 28, pp. 135–145, Jan. 2017, doi: 10.1016/j.scs.2016.09.006.

[35] J. Yang, B. Shi, Y. Shi, S. Marvin, Y. Zheng, and G. Xia, "Air pollution dispersal in high density urban areas: Research on the triadic relation of wind, air pollution, and urban form," *Sustain. Cities Soc.*, vol. 54, Mar. 2020, Art. no. 101941, doi: 10.1016/j.scs.2019.101941.

[36] H. Li, Y. Li, T. Wang, Z. Wang, M. Gao, and H. Shen, "Quantifying 3D building form effects on urban land surface temperature and modeling seasonal correlation patterns," *Building Environ.*, vol. 204, Oct. 2021, Art. no. 108132, doi: 10.1016/j.buildenv.2021.108132.

[37] Z. Liang et al., "The mediating effect of air pollution in the impacts of urban form on nighttime urban heat island intensity," *Sustain. Cities Soc.*, vol. 74, Nov. 2021, Art. no. 102985, doi: 10.1016/j.scs.2021.102985.

[38] L. Li, Z. Zhao, H. Wang, L. Shen, N. Liu, and B.-J. He, "Variabilities of land surface temperature and frontal area index based on local climate zone," *IEEE J. Sel. Topics Appl. Earth Observ. Remote Sens.*, vol. 15, pp. 2166–2174, 2022, doi: 10.1109/JSTARS.2022.3153958.

[39] W. Yu et al., "Attribution of urban diurnal thermal environmental change: Importance of global–Local effects," *IEEE J. Sel. Topics Appl. Earth Observ. Remote Sens.*, vol. 16, pp. 8087–8101, 2023, doi: 10.1109/JSTARS.2023.3308045.

[40] A. Guo et al., "Impact of urban morphology and landscape characteristics on spatiotemporal heterogeneity of land surface temperature," *Sustain. Cities Soc.*, vol. 63, Dec. 2020, Art. no. 102443, doi: 10.1016/j.scs.2020.102443.

[41] X. LiuXue, Y. Ming, Y. Liu, W. Yue, and G. Han, "Influences of landform and urban form factors on urban heat island: Comparative case study between Chengdu and Chongqing," *Sci. Total Environ.*, vol. 820, May 2022, Art. no. 153395, doi: 10.1016/j.scitotenv.2022.153395.

[42] G. Han and J. Xu, "Land surface phenology and Land surface temperature changes along an urban–Rural gradient in Yangtze River Delta, China," *Environ. Manage.*, vol. 52, no. 1, pp. 234–249, Jul. 2013, doi: 10.1007/s00267-013-0097-6.

[43] D. Athukorala and Y. Murayama, "Urban heat island formation in Greater Cairo: Spatio-temporal analysis of daytime and nighttime land surface temperatures along the Urban–Rural gradient," *Remote Sens.*, vol. 13, no. 7, Jan. 2021, Art. no. 7, doi: 10.3390/rs13071396.

[44] Z. Liang et al., "The relationship between urban form and heat island intensity along the urban development gradients," *Sci. Total Environ.*, vol. 708, Mar. 2020, Art. no. 135011, doi: 10.1016/j.scitotenv.2019.135011.

[45] R. Sun, A. Chen, L. Chen, and Y. Lü, "Cooling effects of wetlands in an urban region: The case of Beijing," *Ecological Indicators*, vol. 20, pp. 57–64, Sep. 2012, doi: 10.1016/j.ecolind.2012.02.006.

[46] A. Guo, W. Yue, J. Yang, T. He, M. Zhang, and M. Li, "Divergent impact of urban 2D/3D morphology on thermal environment along urban gradients," *Urban Climate*, vol. 45, Sep. 2022, Art. no. 101278, doi: 10.1016/j.uclim.2022.101278.

[47] Y. Zhang, A. Middel, and B. L. Turner, "Evaluating the effect of 3D urban form on neighborhood land surface temperature using Google Street View and geographically weighted regression," *Landscape Ecol*, vol. 34, no. 3, pp. 681–697, Mar. 2019, doi: 10.1007/s10980-019-00794-y.

[48] N. M. Rajan, P. Neelamegam, and A. J. Thatheyus, "Multiple linear and non-linear regression analyses of various soil and terrain indices with regard to their efficiency in the determination of temporal changes in LST values within Trichy district of Tamil Nadu, India," *Environ Monit Assess*, vol. 194, no. 2, Feb. 2022, Art. no. 138, doi: 10.1007/s10661-022-09796-x.

[49] A. Mathew, S. Sreekumar, S. Khandelwal, and R. Kumar, "Prediction of land surface temperatures for surface urban heat island assessment over Chandigarh city using support vector regression model," *Sol. Energy*, vol. 186, pp. 404–415, Jul. 2019, doi: 10.1016/j.solener.2019.04.001.

[50] W. Zhao, S.-B. Duan, A. Li, and G. Yin, "A practical method for reducing terrain effect on land surface temperature using random forest regression," *Remote Sens. Environ.*, vol. 221, pp. 635–649, Feb. 2019, doi: 10.1016/j.rse.2018.12.008.

[51] Q. Wang, X. Wang, Y. Zhou, D. Liu, and H. Wang, "The dominant factors and influence of urban characteristics on land surface temperature using random forest algorithm," *Sustain. Cities Soc.*, vol. 79, Apr. 2022, Art. no. 103722, doi: 10.1016/j.scs.2022.103722.

[52] T. Chen and C. Guestrin, "XGBoost: A scalable tree boosting system," in *Proc. 22nd ACM SIGKDD Int. Conf. Knowl. Discov. Data Mining*, New York, NY, USA, 2016, pp. 785–794. doi: 10.1145/2939672.2939785.

[53] S. Demir and E. K. Şahin, "Liquefaction prediction with robust machine learning algorithms (SVM, RF, and XGBoost) supported by genetic algorithm-based feature selection and parameter optimization from the perspective of data processing," *Environ Earth Sci*, vol. 81, no. 18, Sep. 2022, Art. no. 459, doi: 10.1007/s12665-022-10578-4.

[54] M. Zamani Joharestani, C. Cao, X. Ni, B. Bashir, and S. Talebiesfandarani, "PM2.5 Prediction based on random forest, XGBoost, and Deep learning using multisource remote sensing data," *Atmosphere*, vol. 10, no. 7, Jul. 2019, Art. no. 7, doi: 10.3390/atmos10070373.

[55] M. Amjad, I. Ahmad, M. Ahmad, P. Wróblewski, P. Kamiński, and U. Amjad, "Prediction of pile bearing capacity using XGBoost algorithm: Modeling and performance evaluation," *Appl. Sci.*, vol. 12, no. 4, Jan. 2022, Art. no. 4, doi: 10.3390/app12042126.

[56] W. Tan, C. Wei, Y. Lu, and D. Xue, "Reconstruction of all-weather daytime and nighttime MODIS Aqua-Terra land surface temperature products using an XGBoost approach," *Remote Sens.*, vol. 13, no. 22, Jan. 2021, Art. no. 22, doi: 10.3390/rs13224723.

[57] J. Zhang et al., "Measuring the critical influence factors for predicting carbon dioxide emissions of expanding megacities by XGBoost," *Atmosphere*, vol. 13, no. 4, Apr. 2022, Art. no. 4, doi: 10.3390/atmos13040599.

[58] H. Sun, X. Li, Y. Guan, S. Tian, and H. Liu, "The evolution of the urban residential space structure and driving forces in the megacity—A case study of Shenyang City," *Land*, vol. 10, no. 10, Oct. 2021, Art. no. 10, doi: 10.3390/land10101081.

[59] J. Dai, J. Li, J. Ju, and C. Wang, "Monitoring and analysis of urban expansion and change in Shenyang based on multi-source and multi-scale satellite imagery," *Mapping Geospatial Inf.*, vol. 45, no. S1, pp. 160–163+167+170, 2022, [Online]. Available: https://kns.cnki.net/KCMS/detail/detail.aspx?dbcode=CJFD&dbname=CJFDLAST2022&filename=DBCH2022S1050&v=

[60] C. D. Elvidge, K. E. Baugh, M. Zhizhin, and F.-C. Hsu, "Why VIIRS data are superior to DMSP for mapping nighttime lights," *APAN Proc.*, vol. 35, Jun. 2013, Art. no. 62, doi: 10.7125/APAN.35.7.

[61] C. D. Elvidge, M. Zhizhin, T. Ghosh, F.-C. Hsu, and J. Taneja, "Annual time series of Global VIIRS Nighttime lights derived from monthly averages: 2012 to 2019," *Remote Sens.*, vol. 13, no. 5, Jan. 2021, Art. no. 5, doi: 10.3390/rs13050922.

[62] J. Yang and X. Huang, "The 30 m annual land cover dataset and its dynamics in China from 1990 to 2019," *Earth Syst. Sci. Data*, vol. 13, no. 8, pp. 3907–3925, Aug. 2021, doi: 10.5194/essd-13-3907-2021.

[63] M. C. Hansen et al., "High-resolution global maps of 21st-century forest cover change," *Science*, vol. 342, no. 6160, pp. 850–853, Nov. 2013, doi: 10.1126/science.1244693.

[64] M. Bondarenko, D. Kerr, A. Sorichetta, and A. Tatem, "Census/projection-disaggregated gridded population datasets, adjusted to match the corresponding UNPD 2020 estimates, for 183 countries in 2020 using built-Settlement Growth Model (BSGM) outputs," University of Southampton, vol. 19, Sep. 2020. doi: 10.5258/SOTON/WP00685.

[65] X. Yu, X. Guo, and Z. Wu, "Land surface temperature retrieval from Landsat 8 TIRS—Comparison between radiative transfer equation-based method, split window algorithm and single channel method," *Remote Sens.*, vol. 6, no. 10, Oct. 2014, Art. no. 10, doi: 10.3390/rs6109829.

[66] J. Cristóbal, J. C. Jiménez-Muñoz, A. Prakash, C. Mattar, D. Skoković, and J. A. Sobrino, "An improved single-channel method to retrieve land surface temperature from the landsat-8 thermal band," *Remote Sens.*, vol. 10, no. 3, Mar. 2018, Art. no. 3, doi: 10.3390/rs10030431.

[67] A. Dwivedi and M. V. Khire, "Application of split- window algorithm to study Urban Heat Island effect in Mumbai through land surface temperature approach," *Sustain. Cities Soc.*, vol. 41, pp. 865–877, Aug. 2018, doi: 10.1016/j.scs.2018.02.030.

[68] Z. Qin, A. Karnieli, and P. Berliner, "A mono-window algorithm for retrieving land surface temperature from Landsat TM data and its application to the Israel-Egypt border region," *Int. J. Remote Sens.*, vol. 22, no. 18, pp. 3719–3746, Jan. 2001, doi: 10.1080/01431160010006971.

[69] O. Conrad et al., "System for Automated Geoscientific Analyses (SAGA) v. 2.1.4," *Geoscientific Model Develop.*, vol. 8, no. 7, pp. 1991–2007, Jul. 2015, doi: 10.5194/gmd-8-1991-2015.

[70] Y. Zhou, C. Li, W. Zheng, Y. Rong, and W. Liu, "Identification of urban shrinkage using NPP-VIIRS nighttime light data at the county level in China," *Cities*, vol. 118, Nov. 2021, Art. no. 103373, doi: 10.1016/j.cities.2021.103373.

[71] Y. Zhou, X. Li, G. R. Asrar, S. J. Smith, and M. Imhoff, "A global record of annual urban dynamics (1992–2013) from nighttime lights," *Remote Sens. Environ.*, vol. 219, pp. 206–220, Dec. 2018, doi: 10.1016/j.rse.2018.10.015.

[72] C. Li, P. Duan, M. Wang, J. Li, and B. Zhang, "The extraction of built-up areas in Chinese mainland cities based on the local optimal threshold method using NPP-VIIRS images," *J Indian Soc Remote Sens*, vol. 49, no. 2, pp. 233–248, Feb. 2021, doi: 10.1007/s12524-020-01209-1.

[73] D. G. Bonett and T. A. Wright, "Sample size requirements for estimating pearson, kendall and spearman correlations," *Psychometrika*, vol. 65, no. 1, pp. 23–28, Mar. 2000, doi: 10.1007/BF02294183.

[74] N. Schwarz, U. Schlink, U. Franck, and K. Großmann, "Relationship of land surface and air temperatures and its implications for quantifying urban heat island indicators—An application for the city of Leipzig (Germany)," *Ecological Indicators*, vol. 18, pp. 693–704, Jul. 2012, doi: 10.1016/j.ecolind.2012.01.001.

[75] J. Li et al., "Application of XGBoost algorithm in the optimization of pollutant concentration," *Atmospheric Res.*, vol. 276, Oct. 2022, Art. no. 106238, doi: 10.1016/j.atmosres.2022.106238.

[76] F. Sun, M. Liu, Y. Wang, H. Wang, and Y. Che, "The effects of 3D architectural patterns on the urban surface temperature at a neighborhood scale: Relative contributions and marginal effects," *J. Cleaner Prod.*, vol. 258, Jun. 2020, Art. no. 120706, doi: 10.1016/j.jclepro.2020.120706.

[77] Z. Wang, Q. Meng, D. Hu, and Y. Zhang, "A deep learning approach of prioritizing influencing factors of land surface temperature," in *Proc. IGARSS 2022 - 2022 IEEE Int. Geosci. Remote Sens. Symp.*, Kuala Lumpur, Malaysia, Jul. 2022, pp. 2351–2354. doi: 10.1109/IGARSS46834.2022.9883774.

[78] R. Shwartz-Ziv and A. Armon, "Tabular data: Deep learning is not all you need," *Inf. Fusion*, vol. 81, pp. 84–90, May 2022, doi: 10.1016/j.inffus.2021.11.011.

[79] X. Zhang, C. Yan, C. Gao, B. A. Malin, and Y. Chen, "Predicting missing values in medical data via XGBoost regression," *J Healthc Inform Res*, vol. 4, no. 4, pp. 383–394, Dec. 2020, doi: 10.1007/s41666-020-00077-1.

[80] O. Rozenstein, Z. Qin, Y. Derimian, and A. Karnieli, "Derivation of land surface temperature for landsat-8 TIRS using a split window algorithm," *Sensors*, vol. 14, no. 4, Apr. 2014, Art. no. 4, doi: 10.3390/s140405768.
[81] C. Yang et al., "Investigating seasonal effects of dominant driving factors on urban land surface temperature in a snow-climate City in China," *Remote Sens.*, vol. 12, no. 18, Jan. 2020, Art. no. 18, doi: 10.3390/rs12183006.
[82] J. Peng, J. Jia, Y. Liu, H. Li, and J. Wu, "Seasonal contrast of the dominant factors for spatial distribution of land surface temperature in urban areas," *Remote Sens. Environ.*, vol. 215, pp. 255–267, Sep. 2018, doi: 10.1016/j.rse.2018.06.010.
[83] Z. Cai, G. Han, and M. Chen, "Do water bodies play an important role in the relationship between urban form and land surface temperature?," *Sustain. Cities Soc.*, vol. 39, pp. 487–498, May 2018, doi: 10.1016/j.scs.2018.02.033.
[84] L. Chen, X. Wang, X. Cai, C. Yang, and X. Lu, "Seasonal variations of daytime land surface temperature and their underlying drivers over Wuhan, China," *Remote Sens.*, vol. 13, no. 2, Jan. 2021, Art. no. 2, doi: 10.3390/rs13020323.
[85] W. Wu, L. Li, and C. Li, "Seasonal variation in the effects of urban environmental factors on land surface temperature in a winter city," *J. Cleaner Prod.*, vol. 299, May 2021, Art. no. 126897, doi: 10.1016/j.jclepro.2021.126897.
[86] Z. Zhang, W. Luan, J. Yang, A. Guo, M. Su, and C. Tian, "The influences of 2D/3D urban morphology on land surface temperature at the block scale in Chinese megacities," *Urban Climate*, vol. 49, May 2023, Art. no. 101553, doi: 10.1016/j.uclim.2023.101553.
[87] D. Bera, N. D. Chatterjee, S. Ghosh, S. Dinda, and S. Bera, "Recent trends of land surface temperature in relation to the influencing factors using Google Earth Engine platform and time series products in megacities of India," *J. Cleaner Prod.*, vol. 379, Dec. 2022, Art. no. 134735, doi: 10.1016/j.jclepro.2022.134735.
[88] J. Yang, Y. Yang, D. Sun, C. Jin, and X. Xiao, "Influence of urban morphological characteristics on thermal environment," *Sustain. Cities Soc.*, vol. 72, Sep. 2021, Art. no. 103045, doi: 10.1016/j.scs.2021.103045.
[89] W. Jia and S. Zhao, "Trends and drivers of land surface temperature along the urban-rural gradients in the largest urban agglomeration of China," *Sci. Total Environ.*, vol. 711, Apr. 2020, Art. no. 134579, doi: 10.1016/j.scitotenv.2019.134579.
[90] Y. Yang, S. Guangrong, Z. Chen, S. Hao, Z. Zhouyiling, and Y. Shan, "Quantitative analysis and prediction of urban heat island intensity on urban-rural gradient: A case study of Shanghai," *Sci. Total Environ.*, vol. 829, Jul. 2022, Art. no. 154264, doi: 10.1016/j.scitotenv.2022.154264.
[91] J. Yuan, Z. Bian, Q. Yan, Z. Gu, and H. Yu, "An approach to the temporal and spatial characteristics of vegetation in the growing season in western China," *Remote Sens.*, vol. 12, no. 6, Jan. 2020, Art. no. 6, doi: 10.3390/rs12060945.
[92] Y. Zhang et al., "Study on the spatial variation of China's territorial ecological space based on the standard deviation ellipse," *Front. Environ. Sci.*, vol. 10, 2022, Accessed: Jun. 30, 2023. [Online]. Available: https://www.frontiersin.org/articles/10.3389/fenvs.2022.982734
[93] Y. Ma, S. Zhang, K. Yang, and M. Li, "Influence of spatiotemporal pattern changes of impervious surface of urban megaregion on thermal environment: A case study of the Guangdong – Hong Kong – Macao Greater Bay Area of China," *Ecological Indicators*, vol. 121, Feb. 2021, Art. no. 107106, doi: 10.1016/j.ecolind.2020.107106.

**Xinyue Ma** received the bachelor's degree in urban planning in 2021 from Jiangho Architecture, Northeastern University, Shenyang, China, where she is currently working toward the master's degree in architecture with the Jiangho Architecture.

Her research interests include urban planning, urban climate, and carbon emissions.

**Jun Yang** received the Ph.D. degree in human geography from Liaoning Normal University, Dalian, China, in 2009.

He is currently a Professor in the effect of human settlement and GIS with Liaoning Normal University, and a Professor of Jiangho Architecture, Northeastern University, Shenyang, China. His research interests include urban space growth, urban thermal environmental, cellular automata land use change, and urban human settlements.

**Rui Zhang** received the bachelor's degree in geographic information science from the School of Geographical Sciences, Liaoning Normal University, Dalian, China, in 2021. She is currently working toward the master's degree in architecture with the Jiangho Architecture, Northeastern University, Shenyang, China.

Her research interests include urban thermal environment, local climate zone, and urban planning.

**Wenbo Yu** is currently working toward the Ph.D. degree in land resources management with Northeastern University, Shenyang, China.

His current research interests include spacetime evolution of human settlements, urban thermal environment, and urban landscape analysis.

**Jiayi Ren** is currently working toward the Ph.D. degree in land resources management with Northeastern University, Shenyang, China. She has been committed to assessment of urban thermal environment and land use policy.

**Xiangming Xiao** received the Ph.D. degree in ecology from Colorado State University, Fort Collins, CO, USA, in 1994.

He is currently a Professor with the School of Atmospheric and Geography, University of Oklahoma, Norman, OK, USA, and the Director of the Earth Observation and Modeling Office. His research interests include land use and land cover change, carbon cycle, and ecological environment analysis of infectious diseases.

**Jianhong Xia** received the Ph.D. degree in geographic information science from Liaoning Normal University, Dalian, China, in 1996.

She has more than ten years' experience as a GIS Educator and Spatial Analyst and Modeler. She was a Transport Geographer and Transit Planner. Her research interests include relation to tourism, public transport development, driving, spatial navigation and way finding and human mobility.